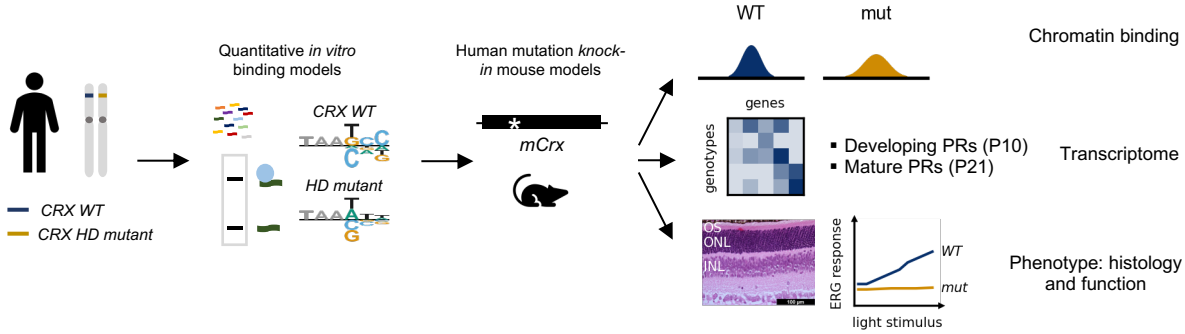

Supplementary Figure S1. Multi-omics approach to investigate the functional consequences of dominant disease mutations on CRX regulatory activities and photoreceptor development.
Human retinopathy associated CRX HD mutant is first tested *in vitro* for HD-DNA interactions by Spec-seq. Quantitative binding models are generated for WT and mutant HDs. Each mutation is then introduced into endogenous *mCrx* locus to generate human mutation knock-in mouse models. ChIP-seq is employed to characterize CRX chromatin binding in *WT* and mutant mouse retinas. Bulk RNA-seq is then applied to determine transcriptomic changes in developing (P10) and mature (P21) photoreceptors in both *WT* and mutant mouse retinas. Last, phenotypic characterization on retinal morphology and visual functions is carried out to understand the consequences of mutant CRX chromatin binding and associated transcriptomic alterations.

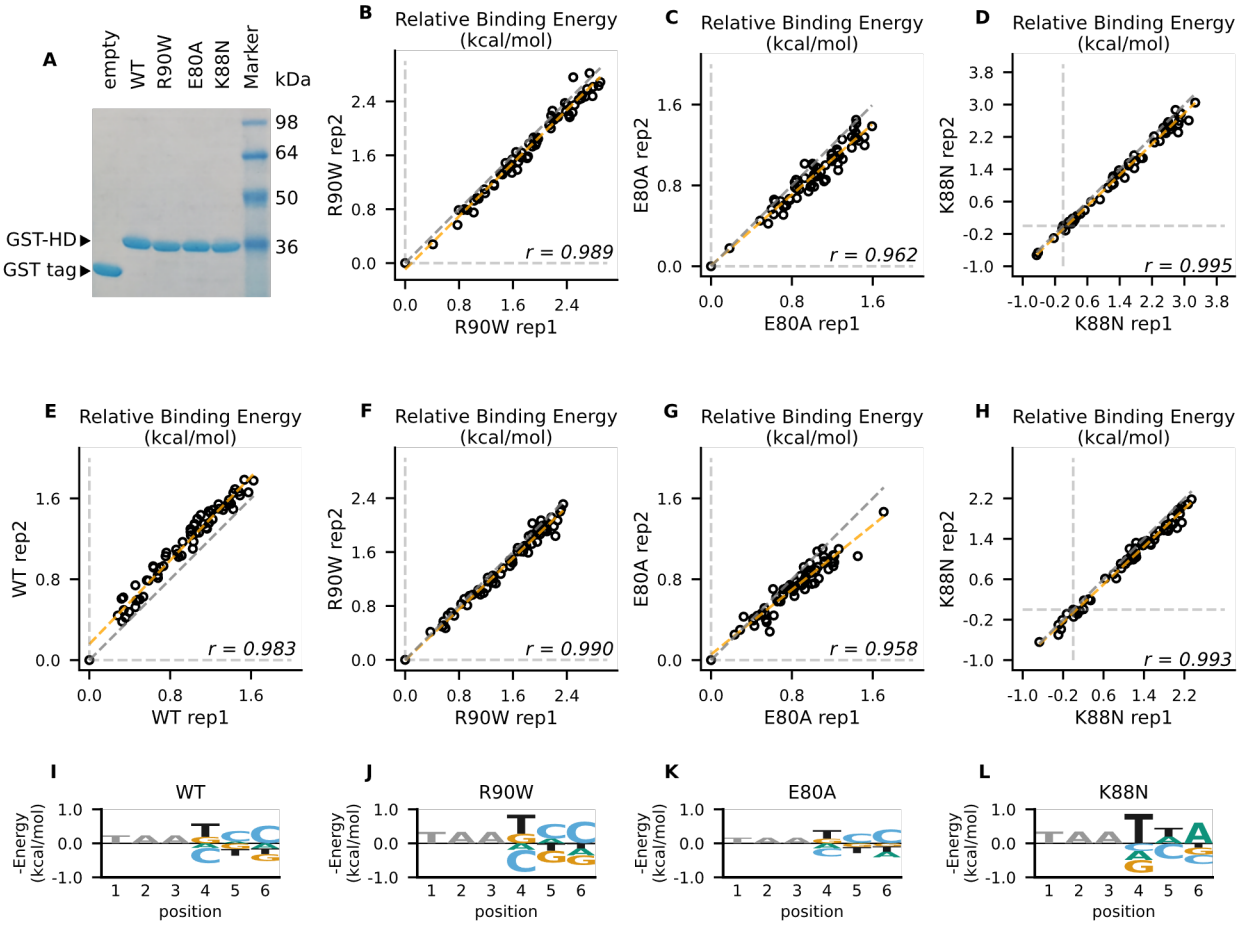

Supplementary Figure S2. Reversed-strand Spec-seq library showed similar changes in mutant CRX HD DNA-binding specificity.
(A) Native SDS-PAGE gel image of affinity purified empty GST tag and GST-CRX HDs.
(B-D) Relative binding energy comparison from two different experiments for R90W HD (B), E80A HD (C), and K88N HD (D) on the same Spec-seq library as in Figure 2.
(E-L) Spec-seq experiments of a second library with the TAANNN sites on the reverse strand show similar results. (E-H) Relative binding energy comparison from two different experiments for WT HD (E), R90W HD (F), E80A HD (G), and K88N HD (H) on the reversed monomeric library. The diagonal line of identity is represented in grey dash. The orange dashed line shows the best linear fit to the data. (I-L) Binding energy models for WT HD (I), R90W HD (J), E80A HD (K), and K88N HD (L) obtained from the reversed monomeric library. Quantitative difference with models obtained from forward-oriented library likely comes from difference in sequences immediately flanking the TAANNN variable region.

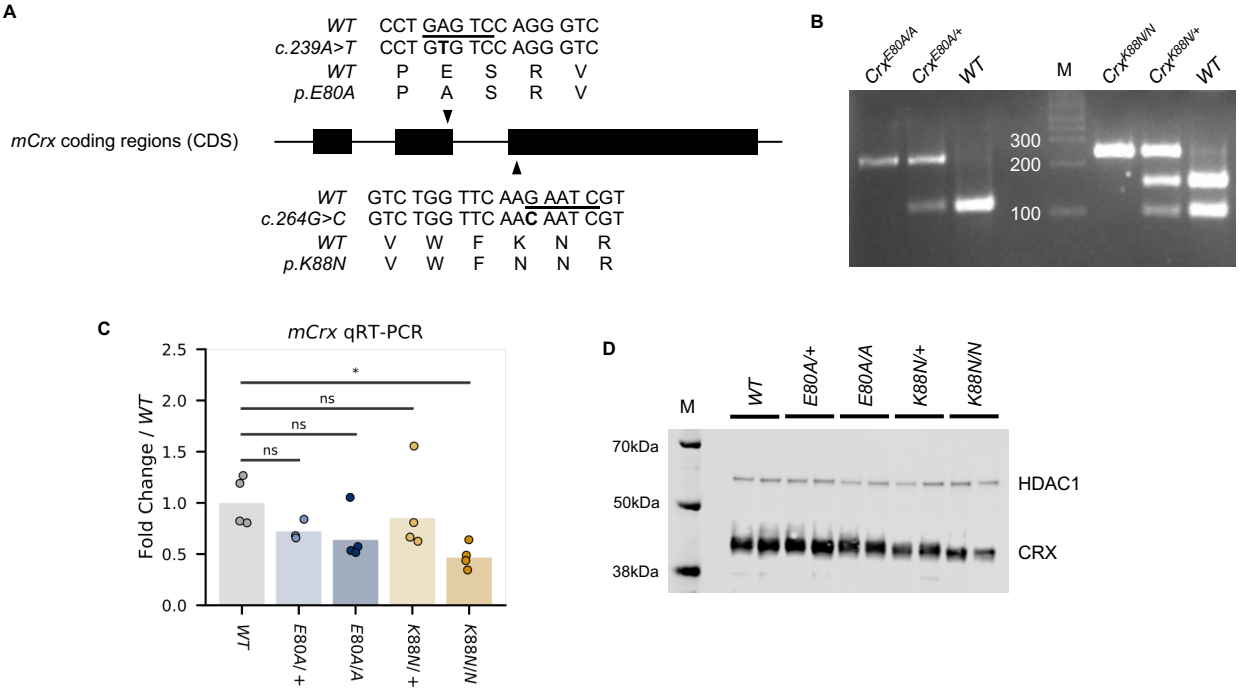

Supplementary Figure S3. WT and mutation knock-in mouse CRX sequences and genotyping identifications
(A) Alignment of *mCrx* cDNA and protein sequences showing the nucleotide substitutions and amino acid changes of Crx^{E80A} (top) and Crx^{K88N} (bottom) alleles. Only coding regions of *mCrx* exons are shown and the diagram is not to scale. Underlined bases in WT sequences indicate the restriction enzyme HinfI cut sites used in the genotyping PCR.
(B) Representative mutation knock-in mouse genotyping gel image.
(C) Barchart and stripplot showing *mCrx* mRNA expression levels in P14 *WT* and mutant mouse retinas. *P-values* for one-way ANOVA with Turkey honestly significant difference (HSD) test are indicated. *p-value*: ****: ≤0.0001, ***: ≤0.001, **: ≤0.01, *: ≤0.05, ns: >0.05.
(D) Immunoblots of nuclear extracts generated from P14 *WT* and mutant mouse retinas showing that full-length CRX protein are produced and localized to the nucleus fraction in all mutant mouse retinas. HDAC1 was used as a loading control.

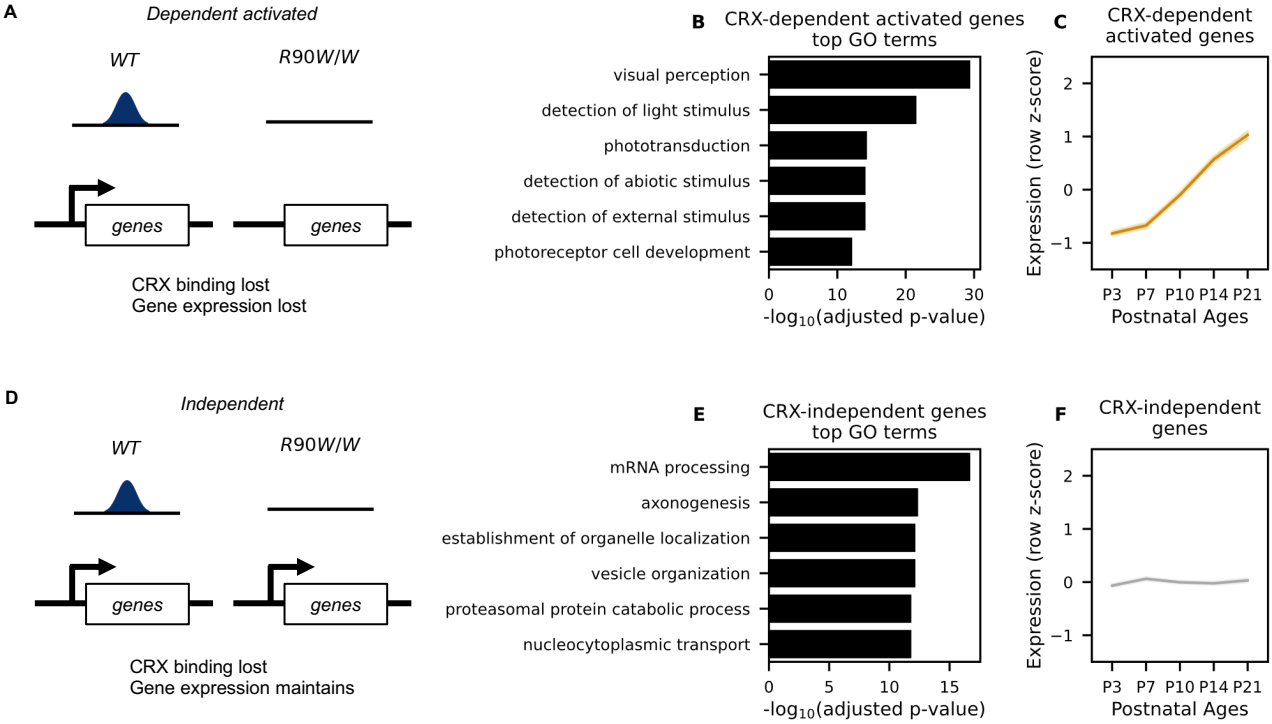

Supplementary Figure S4. Definition of CRX-dependent activated and CRX-independent gene sets.
(A) Schematic representation of CRX-dependent activated genes where CRX binding nearby is required for the expression of these genes in mature *WT* retinas.
(B) Top GO terms associated with CRX-dependent activated genes. Benjamini-Hochberg adjusted p-values are shown.
(C) Line plot showing average expression pattern of CRX-dependent activated genes during normal post-natal retina.
(D) Definition of CRX-independent genes where CRX binding nearby is dispensable for the expression of these genes in mature *WT* retinas.
(E) Top GO terms associated with CRX-independent genes.
(F) Line plot showing average expression pattern of CRX-independent genes during normal retina development. RNA-seq data in (C) and (F) were retrieved from GSE87064.

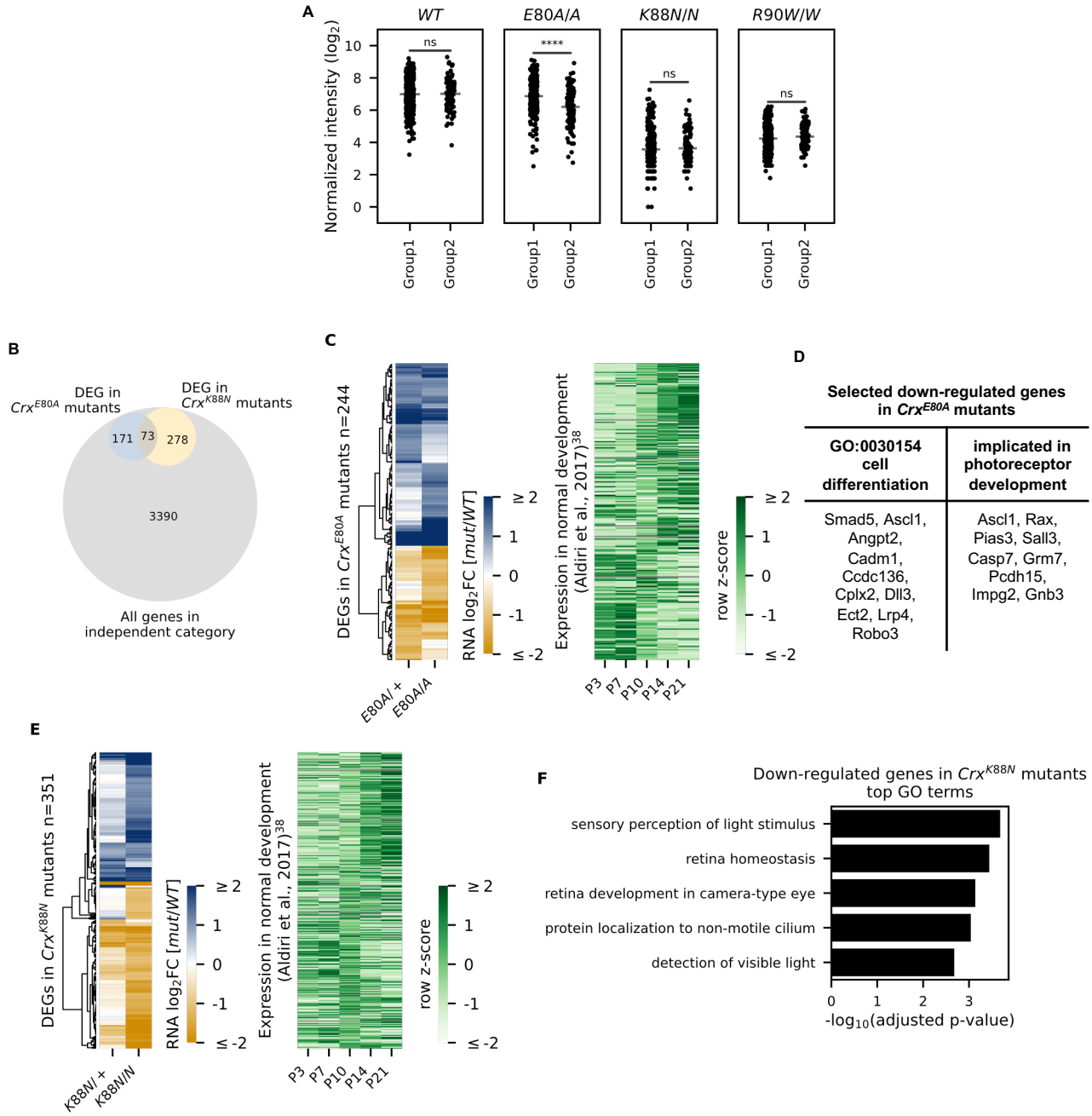

Supplementary Figure S5. E80A and K88N mutation each causes novel gene expression changes in the CRX-independent category

(A) Strip plots showing normalized CRX ChIP-seq intensity at peaks associated with Group1 or Group2 genes in WT and CRX mutant mouse retinas. *P-values* for two-sided Mann-Whitney U test are indicated. *p-value*: ****: ≤0.0001, ***: ≤0.001, **: ≤0.01, *: ≤0.05, ns: >0.05.

(B) Venn diagram showing the overlap of genes differentially expressed (DEGs) in Crx^{E80A} (pale blue) and Crx^{K88N} (pale yellow) but not in $Crx^{R90W/W}$ (grey) mutant retinas. For DEGs in Crx^{E80A} and Crx^{K88N} mutants, genes that were differentially expressed in either heterozygotes or homozygotes, or both were counted.

(C) Heat map showing the expression changes of CRX-independent genes that are DEGs in at least one of the Crx^{E80A} mutants (n = 244, left). Heat map on the right shows the expression pattern of these genes during normal post-natal development (data from GSE87064).

(D) Table showing selected genes down-regulated in Crx^{E80A} mutants that have been implicated in cell differentiation or photoreceptor development.

(E) Heat map showing the expression changes of CRX-independent genes that are DEGs in at least one of the Crx^{K88N} mutants (n = 351, left). Heat map on the right shows the expression pattern of these genes during normal post-natal development (data from GSE87064).

(F) Bar chart showing GO term enrichment of DEGs in Crx^{K88N} mutants.

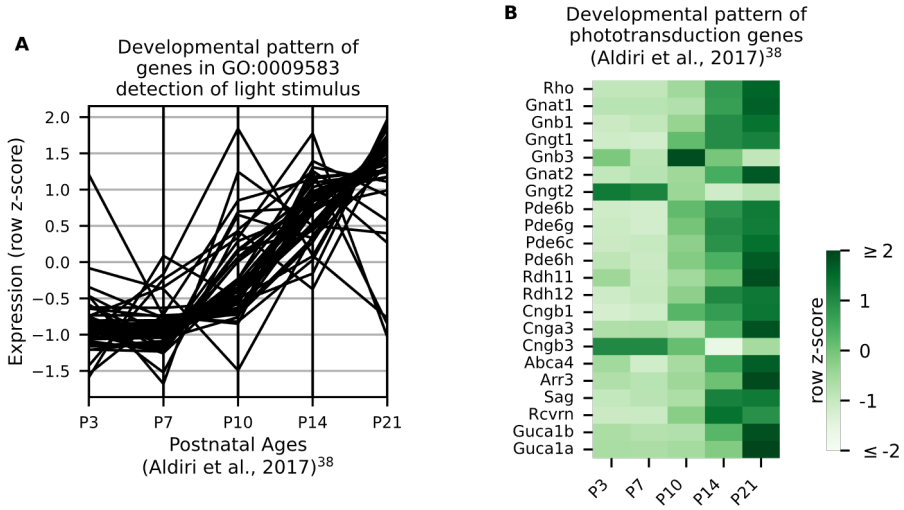

Supplementary Figure S6. Developmental expression pattern of phototransduction genes in *WT* animals

(A) Parallel coordinates plot showing expression pattern of genes in GO:0009583 during normal post-natal retina development (data from GSE87064). Normalized row z-score is shown

(B) Heatmap showing expression patterns of phototransduction genes during normal post-natal retina development (data from GSE87064). Normalized row z-score is shown.